Diffraction imaging of a diatomic molecule using recolliding electrons: Role of Coulomb potential and nuclear motion

A. A. Gonoskov, I. A. Gonoskov, M. Yu. Ryabikin, and A. M. Sergeev
Institute of Applied Physics, Russian Academy of Sciences, 46 Ulyanov Street, Nizhny Novgorod 603950, Russia
(Received 6 December 2007; revised manuscript received 29 February 2008; published 28 March 2008)

We analyze the process of above-threshold ionization (ATI) in light diatomic molecules exposed to an intense linearly polarized femtosecond laser pulse. We concentrate on the problem of extracting high-accuracy dynamic information about the molecular structure from the electron spectra. The results of the frozen-nuclei and moving-nuclei simulations are presented. For a molecule with fixed nuclei, we obtained the corrections to the formula for the interference minima in the electron angular distributions, which improve substantially the determination of the internuclear distance, as confirmed by the comparison with the results of numerical solution of the time-dependent Schrödinger equation (TDSE). To study ATI in molecules with moving nuclei, we used a semiclassical approach in which one solves numerically TDSE for the electron wave function while the nuclear motion is described classically. The influence of a nuclear motion on the electron diffraction images is discussed for the cases of long and few-cycle laser pulses.

DOI: 10.1103/PhysRevA.77.033424 PACS number(s): 33.80.Rv, 34.80.Bm

I. INTRODUCTION

Recent progress in a methodology and technology for the time-resolved measurement of femto- and attosecond dynamics of electrons and nuclei in molecules has marked an emergence of a new branch of ultrashort pulse laser science, molecular ultrafast dynamic imaging (UFDI). In most of the methods for UFDI, the state of the molecule is probed by the electrons which are field ionized, accelerated by the oscillating electric field, and driven back to recollide with the parent molecule (see the recent topical review [1]).

The idea of the molecular dynamic imaging based on an analysis of the photoelectron angular distributions was suggested initially by Zuo *et al.* [2], who proposed to exploit the interference between the de Broglie waves emitted from different centers in a molecule due to the multiphoton ionization. This idea was later extended to the case of using the interference pattern in the electron wave rescattered from the molecular core rather than in the direct electron wave [3,4]. The problem of extracting the internuclear distance from the electron diffraction patterns was addressed in a number of recent theoretical studies [5–8].

A semiclassical approach, which extends the classical analysis of atomic high-order above-threshold ionization (ATI) [9] to molecules by including the two-center interference effects, was proposed in [3] to analyze the angular distributions of ATI electrons scattered by the nuclei in their own molecule. However, as follows from the numerical results presented below, the positions of interference maxima and minima predicted by this simple theory do not match perfectly those provided by the *ab initio* calculations. In Sec. II we present the analytical formulas, which improve significantly the quantitative agreement between the theory and the numerical experiment presented in Sec. III A.

Several physical mechanisms that can distort the recollision-induced diffraction images were pointed out and analyzed in [4]. In Sec. III B we concentrate on the nuclear motion during the probe pulse as one more mechanism that can complicate UFDI using recolliding electrons [10]. Using the semiclassical numerical approach similar to that of [10–12], we study the effect of a nuclear motion on the angular distributions of ATI electrons for both the cases of long and few-cycle laser pulses.

II. HIGH-ORDER ATI: CORRECTION TERMS TO INTERFERENCE MINIMA POSITIONS

The long-range Coulomb forces are known to play a large role in different strong-field laser-molecule interactions. The Coulomb continuum effects in photoionization of molecules [13] and high-order harmonic generation in molecular systems [14] have been examined recently and shown to influence significantly the molecular interference in these processes. Below we study the influence of the Coulomb potential on the high-order ATI electrons angular distributions in the problem of laser-assisted electron rescattering from the parent core in molecular ATI.

A simple semiclassical model was introduced in [3] in order to analyze the electron angular distributions in high-order ATI of molecules in intense linearly polarized laser field. This model extends the classical model, which was applied in [9] to the analysis of the rescattering effects in atomic ATI, by including the interference of electron wave packets scattered from different nuclei in a molecule. In the present paper we modify this model by taking into account the phase corrections caused by the Coulomb potential of the neighboring nuclei in a molecule and, for the two-dimensional (2D) case, the corrections provided by a more accurate consideration of the effective combined potential of two nuclei. Atomic units ($\hbar=m=e=1$) are used throughout the paper.

We assume that the internuclear distance is quite small, so that we can consider the recolliding electron wave packet as a single whole. More definitely, the internuclear distance is considered to be much smaller than the size of the packet and the scale of the electron motion before rescattering.

Let us consider the electron rescattering in a diatomic molecule in the context of the semiclassical model similar to

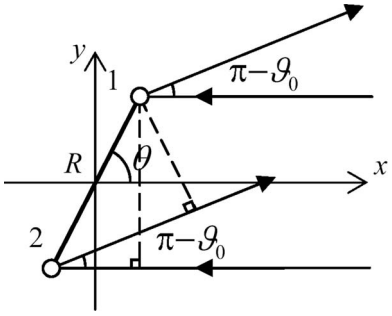

FIG. 1. Scheme of the electron elastic rescattering process in a diatomic molecule driven by a linearly polarized laser field. Leftward arrows depict the electron plane wave returning to the core. The molecular axis is aligned at an angle θ with respect to the polarization axis of a laser field (R is the distance between nuclei 1 and 2). The electron wave is assumed to be scattered from the core by an angle ϑ_0.

that of [3]. The classical equation of motion for the electron in a sinusoidal electric field is $\ddot{x}=-E_0 \sin(\omega_0 t)$. Suppose that ionization happening at the field phase ϕ creates an electron at $x=0$ with zero initial velocity. If we assume that after ionization the electron trajectory is governed by the laser field only, the time τ after which an electron will return to the origin satisfies an equation

$$(\omega_0\tau - \sin\omega_0\tau)\cos\phi = (\cos\omega_0\tau - 1)\sin\phi. \tag{1}$$

The electron returns with a velocity

$$v = (E_0/\omega_0)(\cos\phi' - \cos\phi), \tag{2}$$

where $\phi'=\omega_0\tau+\phi$ is the phase of the field at the time of return. Below we consider the electron rescattering process in a molecule with internuclear distance R, which is oriented at an angle θ with respect to the electric field of the linearly polarized laser pulse (Fig. 1).

We further assume that the returning electron is scattered elastically by an angle ϑ_0. Then at infinity the electron will have the velocity components

$$\dot{x}_f = v\cos\vartheta_0 - (E_0/\omega_0)\cos\phi', \tag{3}$$

$$\dot{y}_f = v\sin\vartheta_0. \tag{4}$$

From Eqs. (3) and (4) the angle at which the electron leaves the pulse can be found: $\alpha(\phi,\vartheta_0)=\arctan(\dot{y}_f/\dot{x}_f)$. The total phase difference due to the difference in the positions of the nuclei with respect to the phase fronts of the returning and scattered electron waves is

$$\Delta\varphi = \Phi(v,R,\theta) + \Phi(v,R,\theta+\vartheta_0-\pi), \tag{5}$$

where the first and the second terms are the phase differences for the incoming and outgoing parts of the electron trajectory, respectively. In the simplest case that the electron is considered to interact with one nucleus only (which it scatters from) and the interaction potential is zero range, one has

$$\Phi(v,R,\beta) = vR\cos\beta, \tag{6}$$

as in [3] [to calculate the first and second contributions to $\Delta\varphi$ in Eq. (5), one should put the angle β in Eq. (6) to θ and $\theta+\vartheta_0-\pi$, respectively]. However, as will be shown below, this approximation leads to a noticeable disagreement with the results of numerical experiments on the model diatomic molecule described by the sum of two Coulomb-like potentials. If we take into consideration the attractive tails of the potentials of two nuclei, we obtain

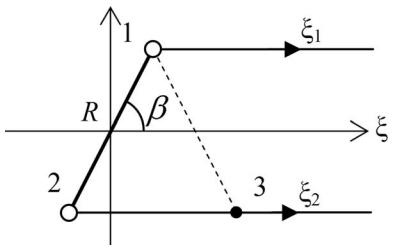

FIG. 2. Schematic picture illustrating the calculation of the phase difference $\Phi(v,R,\beta)$. For the recolliding electron $\beta=\theta$ and $\xi=x$, while for the rescattered electron $\beta=\theta+\vartheta_0-\pi$ and ξ is the coordinate parallel to the asymptote of the electron trajectory at infinity. $\Delta 123$ is isosceles triangle with $l_{12}=l_{13}=R$.

$$\Phi(v,R,\beta) = vR\cos\beta + \int_0^\infty \sqrt{v^2 - 2V(\xi_2) - 2G_1^2(\xi_2)}\,d\xi_2 - \int_0^\infty \sqrt{v^2 - 2V(\xi_1) - 2G_2^1(\xi_1)}\,d\xi_1, \tag{7}$$

where $V(\xi)$ is the potential of the scattering center, $G_i^k(\xi_k)$ is the potential of the ith nucleus on the line passing through the kth nucleus, and ξ_i is the coordinate along the asymptote of the trajectory of the electron hitting the ith nucleus or scattered from it (see Fig. 2).

Since we will be interested hereafter in the scattering of high-energy electrons, for which $|V(\xi_k)|, |G_i^k(\xi_k)| \ll v^2/2$, we can expand the integrals in Eq. (7) and obtain

$$\Phi(v,R,\beta) = vR\cos\beta - \frac{1}{v}\left(\int_0^\infty G_1^2(\xi_2)\,d\xi_2 - \int_0^\infty G_2^1(\xi_1)\,d\xi_1\right). \tag{8}$$

Seeing that $\int_{X_3}^\infty G_1^2(\xi_2)d\xi_2 = \int_0^\infty G_2^1(\xi_1)d\xi_1$, where $X_3=2R\cos\beta$ is the coordinate of the point 3 in Fig. 2, we obtain

$$\Phi(v,R,\beta) = vR\cos\beta - \frac{2}{v}\int_0^{R\cos\beta} V\left(\sqrt{\xi^2 + R^2\sin^2\beta}\right)d\xi. \tag{9}$$

In our 2D numerical simulation presented in Sec. III we used a smoothed Coulomb potential $V(r)=-(r^2+a^2)^{-1/2}$ for each center, which is a common choice for the atomic and molecular models of reduced dimensionality [15–17]. Integration of Eq. (9) with this potential gives

$$\Phi(v,R,\beta) = vR\cos\beta + \frac{2}{v}\ln\left(\frac{R\cos\beta + \sqrt{R^2+a^2}}{\sqrt{R^2\sin^2\beta + a^2}}\right). \tag{10}$$

For the real 3D case ($a=0$), one can obtain from Eq. (7) the upper estimate for $\Phi(v,R,\beta)$ for high-energy electrons.

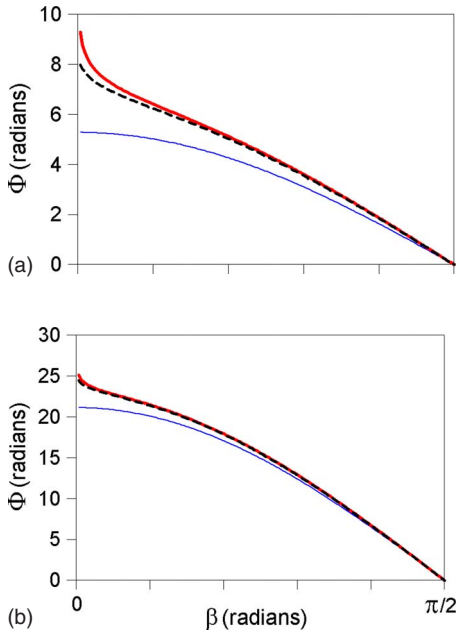

FIG. 3. (Color online) Phase difference $\Phi(v,R,\beta)$ [$v=2.62$; $R=2$ (a) and $R=8$ (b)] as a function of β calculated for 3D case using Eq. (11) (thick solid line), simple theory [3], i.e., the first term in Eq. (10) (thin solid line), and the exact numerical integration of Eq. (7) with the Coulomb potential (dashed line).

Neglecting a small contribution from a short part of the trajectory where $|V(\xi_k)| \geqslant v^2/2$, one has

$$\Phi(v,R,\beta) = vR\cos\beta + \frac{2}{v}\ln\left(\frac{\cos\beta+1}{\sin\beta}\right), \tag{11}$$

which is just what could be obtained from Eq. (10) by simply putting a to zero.

We should mention that Eq. (11) is identical to the result derived in [13,14] for the cases of direct photoionization and high-order harmonic generation, respectively. The coincidence could be explained by the fact that, although our calculation is technically different, the approach we use is conceptually equivalent to that of [13,14], since basically it also uses the eikonal approximation [18] (see also [19]) that is justified for the scattering of high-energy particles. We note also that, although the logarithmic shift in Eq. (11) does not depend or R, it modifies the two-center interference pattern and, hence, can affect significantly the link between the positions of the interference minima and the molecular structure extracted from this pattern.

Figure 3 provides a comparison of the phase difference $\Phi(v,R,\beta)$ for a 3D case given by the formula (11) with that calculated using the simple theory [3] and the exact numerical integration of Eq. (7) with the Coulomb potential. The results are shown for the case $v=2.62$, which corresponds to the highest velocity of the returning electron for the laser parameters used in Fig. 5 and Sec. III A. It is clearly seen from Fig. 3 that Eq. (11) appears to be good estimation for all β, except for a small vicinity of $\beta=0$. The agreement can be shown to be more close for higher v and larger R.

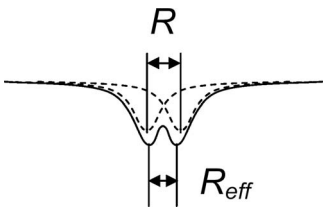

FIG. 4. The positions of effective scattering centers.

Since a full-dimensionality *ab initio* calculation of the angle-resolved ATI spectrum is a formidable task, we will test our modified semiclassical model using a 2D numerical simulation. For that purpose we will further modify our model for the 2D case by including the correction to the phase difference that is caused by the fact that in the 2D potential of two nuclei

$$V(x,y) = V_1(x,y) + V_2(x,y) = -1/\sqrt{(x-R/2)^2+y^2+a^2} - 1/\sqrt{(x+R/2)^2+y^2+a^2} \tag{12}$$

the distance between minima, which can be regarded as the separation of effective positions of the scattering centers, is a little smaller than R (Fig. 4). This fact means that in Eq. (10) we should use $R_{eff}(R)$ instead of R. To explain the derivation of $R_{eff}(R)$, we first consider a 1D parabolic potential $V(x')=\alpha x'^2$, which approximates at the $y=0$ plane the potential $-[(x-R/2)^2+y^2+a^2]^{-1/2}$ near the minimum. It is symmetric with the center at $x'=0$. If we add a uniform field, the resulting potential $\alpha x'^2-\gamma x'=\alpha[x'-\gamma/(2\alpha)]^2-\gamma^2/(4\alpha)$ has the center of symmetry shifted by the distance $\Delta x'=\gamma/(2\alpha)$. To obtain $R_{eff}(R)$, one should take γ from the linear approximation of the neighboring nucleus potential.

We suppose that the positions of the effective scattering centers coincide with the positions of potential minima. Taking into account the first two terms of the Taylor series expansion of $V_2(x)$ and calculating the derivative of the potential $V_1(x)$ of the neighboring nucleus, we obtain the absolute value for the shift

$$\Delta x = a^3 \left.\frac{x+R/2}{[(x+R/2)^2+a^2]^{3/2}}\right|_{x=R/2}. \tag{13}$$

We thus have for $R_{eff}=R-2\Delta x$,

$$R_{eff} = R\left[1-\frac{2a^3}{(R^2+a^2)^{3/2}}\right]. \tag{14}$$

Using Eq. (5) with Eqs. (10) and (14), one can finally find the total phase difference $\Delta\varphi$, which determines a contribution of any particular electron trajectory taking into account the two-center interference effects through the factor $|1+\exp(i\Delta\varphi)|^2=4\cos^2(\Delta\varphi/2)$. By summing over all ionization times ϕ/ω_0 and scattering angles ϑ_0 we can then calculate the angular distributions of ATI electrons at different energies.

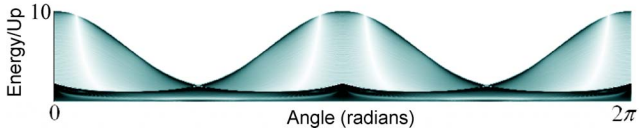

FIG. 5. (Color online) Angle-resolved ATI spectrum for H_2^+ with internuclear distance $R=2.62$ a.u., aligned perpendicular to the laser field. The spectrum was calculated using the modified semiclassical model. The laser field strength and angular frequency are $E_0=0.12$ a.u. ($I=5\times10^{14}$ W cm^{-2}) and $\omega_0=0.057$ a.u. ($\lambda=800$ nm), respectively, yielding $U_p=E_0^2/4\omega_0^2 \approx 1.1$ a.u.

Figure 5 shows the angle-resolved ATI spectrum calculated using our modified semiclassical model in a range of electron energies from 0 to $10U_p$ for H_2^+ ion aligned perpendicular to the laser field. The internuclear distance was set equal to its equilibrium value for the 2D model with $a=1/\sqrt{2}$ ($R=2.62$ a.u.); the common assumption of a uniform distribution of ionization times and scattering angles was made and multiple returns of electrons were neglected, as in [3].

Energy-dependent interference minima (light regions on the contour plot in Fig. 5) are clearly seen on the angle-resolved ATI spectrum. From the locations of angles of destructive interference, the information on the molecular structure can be extracted using the analytical formulae presented above.

It can be seen in Fig. 5 that for each angle α at the detector the electron energy does not exceed the maximum value $W_{\max}(\alpha)$. As follows from the numerical analysis of the classical equation of motion, for $\alpha=\pi$ this cutoff energy is $W_{\max}(\pi)\approx 10.007U_p$ [9]; the corresponding phases of the field at the instants of the electron's release and first return are, respectively, $\phi_{\max}\approx 1.83$ and $\phi'_{\max}\approx 3.06$.

For the electron born at $\phi=\phi_{\max}$ the velocity upon the first return is $v_1=(E_0/\omega_0)(\cos\phi'_{\max}-\cos\phi_{\max}) \approx 1.25(E_0/\omega_0)$; the final velocity is determined by Eqs. (3) and (4). For any other angle α the electron's maximal energy can be found as

$$W_{\max}(\alpha)=\tfrac{1}{2}[v_1^2+v_p^2-2v_1v_p\cos\vartheta(\alpha)], \tag{15}$$

where $v_p=(E_0/\omega_0)\cos\phi'_{\max}\approx 0.988(E_0/\omega_0)$; the function $\vartheta(\alpha)$ is the solution of the equation

$$\tan\alpha=\frac{v_1\sin\vartheta}{v_1\cos\vartheta-v_p}. \tag{16}$$

Below we will concentrate on the positions of interference minima of the probability distribution along the curve $W_{\max}(\alpha)$. The internuclear distance can be deduced from the implicit formula, which expresses the conditions for the two-center destructive interference,

$$\Delta\varphi[v_1,R_{eff}(R),\vartheta(\alpha^n_{\min})]=\frac{\pi}{2}+n\pi, \tag{17}$$

where n are positive integers.

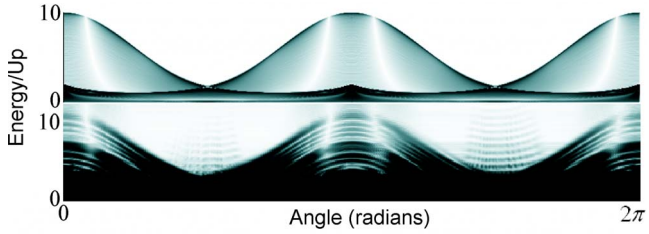

FIG. 6. (Color online) Angle-resolved ATI spectra for H_2^+ with internuclear distance $R=2.62$ a.u., aligned perpendicular to the laser field. Lower case: The spectrum calculated using the numerical solution of TDSE. The laser pulse is trapezoidal with three-cycle linear ramps and four-cycle flat top of amplitude $E_0=0.12$ a.u.; the laser angular frequency is $\omega_0=0.057$ a.u. The solution for the time interval between $t=4T$ and $t=5T$ (T is the laser cycle) was used. Upper case: The spectrum calculated using our modified semiclassical model (see the caption to Fig. 5).

III. NUMERICAL SIMULATION

A. Frozen-nuclei approximation

In this section we present the *ab initio* calculation of the angle-resolved spectra of ATI electrons from a diatomic molecular ion in a linearly polarized laser field. In our numerical simulation we use a two-dimensional model of H_2^+. The time evolution of the electron wave function $\psi(x,y,t)$ in the dipole approximation and in the length gauge obeys the TDSE

$$i\frac{\partial\psi}{\partial t}=-\frac{1}{2}\Delta\psi+U(\mathbf{r},t)\psi, \tag{18}$$

where $U(\mathbf{r},t)=V(\mathbf{r})-\mathbf{r}\cdot\mathbf{E}(t)$; $V(\mathbf{r})=-[(\mathbf{r}-\mathbf{R}_1)^2+a^2]^{-1/2}-[(\mathbf{r}-\mathbf{R}_2)^2+a^2]^{-1/2}$ is the molecular potential, $\mathbf{R}_1$ and $\mathbf{R}_2$ are the positions of the nuclei, which we assume here to be fixed, and $\mathbf{E}$ is the electric field of the laser pulse. The smoothing parameter a is set equal to $1/\sqrt{2}$ in order to reproduce the H_2^+ ionization potential and dissociation energy.

We solved Eq. (18) on a 2D grid using the split-operator method [20]. In order to suppress efficiently the reflections of the electron waves of different lengths from the numerical grid boundaries, we used the approach proposed by us recently [21] that provides absorption of any wave whose length is small enough in comparison with the size of the absorption region. To carry out the computation on a large grid, we used an oscillating coordinate frame and applied the division of the configuration space into two parts. In the first (inner) part, which is closer to the nuclei, we solved numerically the TDSE (18). In the second (outer) part the electron-nuclei interaction is negligible, and we used the procedure that maps the solution for the wave function at the boundaries of the inner region onto an arbitrary rectangular surface in the outer part. The solution for the wave function at the boundaries of the outer region was then used to calculate the angle-resolved electron spectra.

The result of a numerical simulation for the case of perpendicular alignment of a molecule is shown in Fig. 6 (lower case). The laser pulse is trapezoidal with three-cycle linear ramps and four-cycle interval of constant amplitude $E_0=0.12$ a.u.; the laser angular frequency is $\omega_0=0.057$ a.u. In

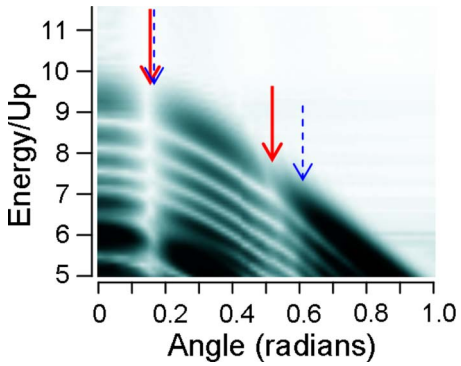

FIG. 7. (Color online) Detailed view of the angle-resolved ATI spectrum calculated numerically for stretched H_2^+ (R=4) aligned perpendicular to the laser field. Arrows show the theoretical positions of the interference minima (n=0, left minimum, and n=1, right minimum) on the high-energy border of the ATI spectrum, according to the simple theory [3] (dashed line) and modified semiclassical model (solid line).

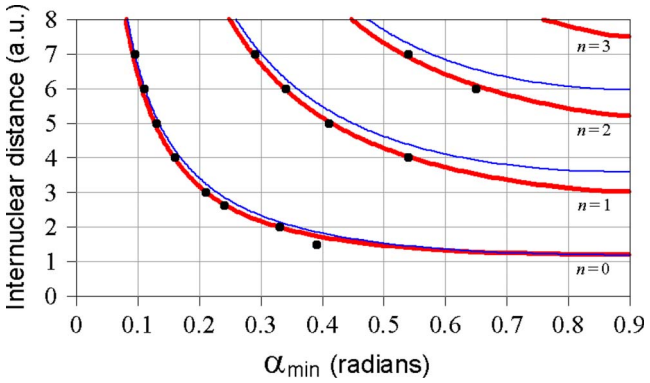

FIG. 8. (Color online) The positions of the interference minima at the angle-dependent cutoff of the ATI spectra depending on the internuclear distance, according to the simple theory [3] (thin line), modified semiclassical model (thick line), and numerical simulation (points). H_2^+ ion is aligned perpendicular to the laser field.

order to make a comparison with the result provided by our modified semiclassical model for the constant-amplitude case (see Fig. 5), we discarded the contribution to the spectrum from the part of the electron wave function which was set free during the rising edge of the pulse. For that we compared the electron spectra calculated separately for each subsequent laser cycle and looked for the moment from which these spectra became stationary. For the case discussed here we found this moment to be equal to four cycles from the beginning of the pulse.

It can be seen that the spectra calculated using the modified semiclassical model (Fig. 6, upper case) and the numerical solution of TDSE (Fig. 6, lower case) agree well in the region of high energies. Although the spectrum in the lower case is somewhat noisy because of imperfections of the numerical scheme, one can easily see the interference minima at the same positions as those predicted by the analytical model. From these minima an information about the internuclear distance can be reliably extracted using our modified semiclassical model.

Figure 7 provides the detailed view of the high-energy region of the angle-resolved ATI spectrum calculated for R =4, where n=0 and n=1 interference minima are clearly seen. The theoretical predictions for the minima positions provided by the model with the Coulomb correction according to Eq. (10) and simple model without Coulomb effects are shown by solid and dashed arrows, respectively. The results clearly illustrate the importance of including the Coulomb effects.

Figure 8 plots the positions of the interference minima of several orders (n=0–3) at the high-energy boundary $W_{max}(\alpha)$ of the angle-resolved ATI spectra. The results obtained using simple theory [3] (thin line), present analytical model (thick line), and numerical simulation (points) are plotted.

The picture confirms that the use of our corrections to the simple formula for the interference minima in the electron angular distributions results in a significant improvement of the determination of the internuclear distance. For example, for the detection angle α=0.21 the inaccuracy of the determination of the internuclear distance from the observation of the n=0 interference minimum in the high-energy electron angular distribution is more than 8% or about 1% if one uses, respectively simple theory [3] or our modified semiclassical model. The relative accuracy of the latter model increases for higher orders of interference (see Fig. 8).

B. Moving-nuclei approximation

In this section we present the results for angle-resolved spectra of ATI electrons from H_2^+ ion obtained taking into account the nuclear motion during the probe pulse. We use the semiclassical numerical approach similar to that of [10–12]. This approach is based on solving the TDSE for the electronic degrees of freedom while the nuclear motion is described classically taking into account the Coulomb attraction experienced by the nuclei from the distributed electron charge. The comparison of the results obtained from this semiclassical and fully quantum calculations has shown [22] the ability of the semiclassical method to provide reliable information about the dynamics of different processes in molecules, including excitation, dissociation, and ionization.

Using the semiclassical method, we described the electron motion by Eq. (18), while the motion of the nuclei was treated classically via the Newton equations:

$$M\frac{d^2\mathbf{R}_1}{dt^2} = \mathbf{E} + \frac{\mathbf{R}_1 - \mathbf{R}_2}{|\mathbf{R}_1 - \mathbf{R}_2|^3} - \int \frac{|\psi(\mathbf{r},\mathbf{R}_1,\mathbf{R}_2,t)|^2}{[(\mathbf{R}_1 - \mathbf{r})^2 + a^2]^{3/2}}(\mathbf{R}_1 - \mathbf{r})d^2\mathbf{r},$$

$$M\frac{d^2\mathbf{R}_2}{dt^2} = \mathbf{E} - \frac{\mathbf{R}_1 - \mathbf{R}_2}{|\mathbf{R}_1 - \mathbf{R}_2|^3} - \int \frac{|\psi(\mathbf{r},\mathbf{R}_1,\mathbf{R}_2,t)|^2}{[(\mathbf{R}_2 - \mathbf{r})^2 + a^2]^{3/2}}(\mathbf{R}_2 - \mathbf{r})d^2\mathbf{r}, \quad (19)$$

where M is the mass of one nucleus. For the case of H_2^+ ion, $M \approx 1836$ a.u.

The propagation of the wave function during one time step Δt was calculated using the formula (see [10])

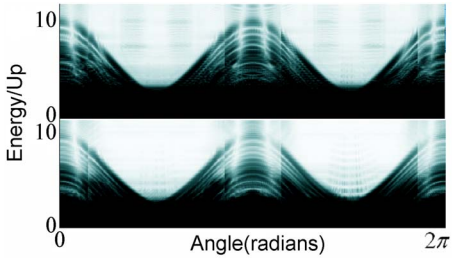

FIG. 9. (Color online) Angle-resolved ATI spectra for H_2^+ with initial internuclear distance $R=2.62$ a.u., aligned perpendicular to the laser field. Upper case: The spectrum calculated taking into account the nuclear motion during the probe pulse. Lower case: The spectrum calculated within the frozen-nuclei approximation. The laser pulse was taken the same as in Fig. 6.

$$\psi(\mathbf{r},\mathbf{R}_1,\mathbf{R}_2,t+\Delta t) = \exp[-\mathrm{i}U(\mathbf{r},t+\Delta t)\Delta t/2]\hat{F}^{-1}\exp(-\mathrm{i}k^2\Delta t/2) \times \hat{F}\exp[-\mathrm{i}U(\mathbf{r},t)\Delta t/2]\times\psi(\mathbf{r},\mathbf{R}_1,\mathbf{R}_2,t)+O(\Delta t^3), \quad (20)$$

where $\mathbf{k}$ is the electron momentum and F is the Fourier transform operator. $U(t+\Delta t)$ is the potential energy with the corrected positions of the nuclei calculated from Eq. (19) after the back Fourier transformation of the wave function into the real space.

Using this method, we calculated the angle-resolved spectra of ATI electrons from H_2^+ for two cases: (i) for the same laser pulse as in the previous section and (ii) for a few-cycle laser pulse $E(t)=E_0\exp(-t^2/\tau^2)\cos\omega_0 t$ with $E_0=0.12$ a.u. and full width at half maximum of intensity (FWHM$=\tau\sqrt{2\ln 2}$) equal to 5 fs.

The results for the 27-fs trapezoidal pulse are presented in Fig. 9. Unlike in Fig. 6, the probability densities time-integrated over the entire pulse are shown in Fig. 9. As the calculation for this rather long pulse shows, the electron spectra calculated taking into account the nuclear motion disagree significantly with those obtained within the frozen-nuclei model. More specifically, for the moving-nuclei case (Fig. 9, upper case) the angular distance between two deepest interference minima at the high-frequency cutoff of the angle-resolved ATI spectra is approximately 19.5°, while for the frozen-nuclei case this distance is about 26° (see Fig. 9, lower case).

This fact can be understood from Fig. 10. As follows from the simulation in moving-nuclei model, the ionization rate, which is known to be strongly dependent on the internuclear distance, grows with time due to dissociation and reaches its maximum value by the beginning of the trailing edge of the pulse. Ionization and recollision events occurring near this time make the dominant contribution to the resulting ATI spectrum.

That is why in the moving-nuclei case (Fig. 9, upper case) we see the minima at the positions corresponding to the internuclear distance larger than the initial value $R=2.62$ a.u. (the difference is about 30%). Thus the nuclear motion during the probe pulse is the mechanism that can indeed complicate reading the diffraction images of light molecules taken with the probe pulses as long as few tens femtoseconds. Note that we address here only the perpendicularly aligned molecules. For smaller orientation angles, ionization and dissociation prove to be even faster (see, e.g., [10]) due to charge resonance enhanced ionization [23,24], therefore, nuclear motion is expected to influence the diffraction images even more strongly for orientation angles closer to 0°. On the other hand, the results for the case of a 5-fs pulse (not shown here) show that the positions of the interference minima differ from those obtained within the frozen-nuclei approximation by no more than 3%. From this we can conclude that the diffraction imaging using recolliding electrons can give a satisfactory estimation of the internuclear distance if one uses few-cycle probe pulses.

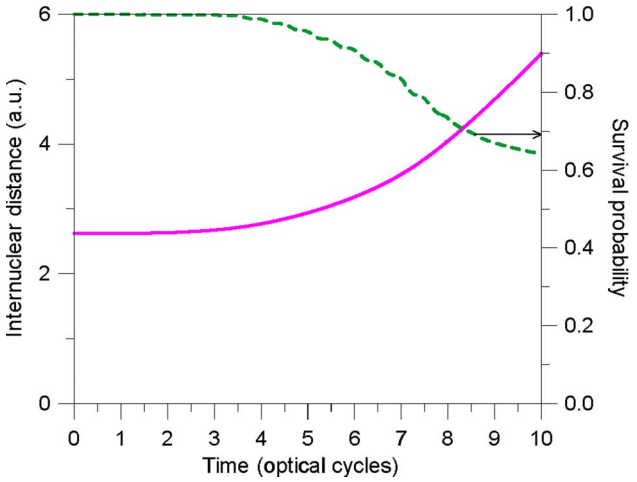

FIG. 10. (Color online) Time dependence of the internuclear distance (solid line) and non-ionized fraction of H_2^+ (dashed line) calculated in moving-nuclei approximation. The laser pulse was taken the same as in Fig. 6.

IV. CONCLUSIONS

In summary, we have analyzed the diffraction of recolliding electrons in a diatomic molecule ionized by femtosecond laser pulse. We aimed at a study of the interference patterns in the angular distributions of high-order ATI electrons. More specifically, for the case of perpendicularly aligned molecules, we concentrated on the positions of interference minima in these distributions as the observable variable used for the diffraction imaging. The positions of these interference minima depend on the phase difference between different parts of the electron wave packet contributing to the yield at particular electron energy for the particular detection angle. We have analyzed the influence of long-range nuclear potential on this phase difference. According to our analysis, taking into account the Coulomb potential of the nuclei allows one to increase the relative accuracy of the determination of the internuclear distance by order of magnitude.

Another important effect that can modify the ATI spectra of light molecule is nuclear motion during the probe pulse. Using a semiclassical numerical simulation, we have shown that in laser pulse with 5×10^{14} W cm^{-2} peak intensity and

30 fs duration the nuclear motion in H_2^+ ion leads to a significant change of the interference minima positions. Due to this effect, in the long-pulse case the extracted internuclear distance can differ by several tens percent from its value before probing. For the case of few-cycle probe pulse the measurement is shown to be almost nonperturbing.

ACKNOWLEDGMENTS

We acknowledge financial support from the Presidium of RAS, RFBR (Grant No. 05-02-17523), and the Russian President's Grant No. 7738.2006.2. A.A.G. and I.A.G. also acknowledge support from the Dynasty Foundation.

[1] M. Lein, J. Phys. B **40**, R135 (2007).
[2] T. Zuo, A. D. Bandrauk, and P. B. Corkum, Chem. Phys. Lett. **259**, 313 (1996).
[3] M. Lein, J. P. Marangos, and P. L. Knight, Phys. Rev. A **66**, 051404R (2002).
[4] M. Spanner, O. Smirnova, P. B. Corkum, and M. Yu. Ivanov, J. Phys. B **37**, L243 (2004).
[5] F. Lepine, S. Zamith, A. de Snaijer, C. Bordas, and M. J. J. Vrakking, Phys. Rev. Lett. **93**, 233003 (2004).
[6] S. X. Hu and L. A. Collins, Phys. Rev. Lett. **94**, 073004 (2005).
[7] A. M. Popov, O. V. Tikhonova, and E. A. Volkova, J. Mod. Opt. **54**, 1087 (2007).
[8] H. Hetzheim, C. Figueira de Morisson Faria, and W. Becker, Phys. Rev. A **76**, 023418 (2007).
[9] G. G. Paulus, W. Becker, W. Nicklich, and H. Walther, J. Phys. B **27**, L703 (1994).
[10] I. A. Gonoskov, M. Yu. Ryabikin, and A. M. Sergeev, J. Phys. B **39**, S445 (2006).
[11] B. Rotenberg, R. Taïeb, V. Véniard, and A. Maquet, J. Phys. B **35**, L397 (2002).
[12] P. P. Corso, R. Daniele, E. Fiordilino, J. P. Marangos, F. Morales, and R. Velotta, Phys. Rev. A **70**, 053410 (2004).
[13] G. L. Yudin, S. Chelkowski, and A. D. Bandrauk, J. Phys. B **39**, L17 (2006).
[14] M. F. Ciappina, C. C. Chirilă, and M. Lein, Phys. Rev. A **75**, 043405 (2007).
[15] J. Javanainen, J. H. Eberly, and Q. Su, Phys. Rev. A **38**, 3430 (1988).
[16] K. C. Kulander, F. H. Mies, and K. J. Schafer, Phys. Rev. A **53**, 2562 (1996).
[17] D. J. Lappas and J. P. Marangos, J. Phys. B **33**, 4679 (2000).
[18] L. D. Landau and E. M. Lifschitz, in *Quantum Mechanics*, 3rd ed. (Pergamon Press, Oxford, 1977), Sec. 131.
[19] S. Selstø, J. F. McCann, M. Førre, J. P. Hansen, and L. B. Madsen, Phys. Rev. A **73**, 033407 (2006).
[20] J. A. Fleck, Jr., J. R. Morris, and M. D. Feit, Appl. Phys. **10**, 129 (1976); M. D. Feit, J. A. Fleck, Jr., and A. Steiger, J. Comput. Phys. **47**, 412 (1982).
[21] A. A. Gonoskov and I. A. Gonoskov, e-print arXiv:physics/0607120.
[22] C. Ruiz, L. Plaja, R. Taïeb, V. Véniard, and A. Maquet, Phys. Rev. A **73**, 063411 (2006).
[23] T. Zuo and A. D. Bandrauk, Phys. Rev. A **52**, R2511 (1995).
[24] T. Seideman, M. Yu. Ivanov, and P. B. Corkum, Phys. Rev. Lett. **75**, 2819 (1995).